이학석사학위논문

Structural and biochemical studies reveal a putative FtsZ recognition site on the Z-ring stabilizer ZapD

2017 년 8 월

서울대학교 대학원

화학과 생화학전공

최 화 정

Structural and biochemical studies reveal a putative FtsZ recognition site on the Z-ring stabilizer ZapD

Thesis by

Hwajung Choi

Professor: Hyung Ho Lee

A Thesis Submitted to the Graduate Faculty of Seoul National University in Partial Fulfillment of the Requirements for the Degree of Master of Science

2017

Abstract

FtsZ, a tubulin homologue, is an essential protein of the Z-ring assembly in bacterial cell division. It consists of two domains, the N-terminal and C-terminal core domains, and has a conserved C-terminal tail region. Lateral interactions between FtsZ protofilaments and several Z-ring associated proteins (Zaps) are necessary for modulating Z-ring formation. ZapD, one of the positive regulators of Z-ring assembly, directly binds to the C-terminal tail of FtsZ and promotes stable Z-ring formation during cytokinesis. To gain structural and functional insights into how ZapD interacts with the C-terminal tail of FtsZ, we solved two crystal structures of ZapD proteins from Salmonella typhimurium (StZapD) and Escherichia coli (EcZapD) at a 2.6 and 3.1 Å resolution, respectively. Several conserved residues are clustered on the concave sides of the StZapD and EcZapD dimers, the suggested FtsZ binding site. Modeled structures of EcZapD-EcFtsZ and subsequent binding studies using bio-layer interferometry also identified the EcFtsZ binding site on EcZapD. The structural insights and the results of bio-layer interferometry assays suggest that the two FtsZ binding sites of ZapD dimer might be responsible for the binding of ZapD dimer to two protofilaments to hold them together.

Keywords: cell division / cytokinesis / FtsZ / ZapD

Student Number: 2015-20416

Contents

List of Figures

List of Table

I. Introduction

In bacterial cell division, cytokinesis is performed by a multi-protein complex called the divisome, which is composed of at least nine proteins (FtsA, FtsI, FtsK, FtsL, FtsN, FtsQ, FtsW, FtsZ, and ZipA) (Margolin, 2000). FtsZ, a tubulin homolog, has a significant role in initiating divisome assembly by forming an organized polymer called the FtsZ ring (Z-ring), which then recruits other division proteins (Pichoff and Lutkenhaus, 2002). The Z-ring can be mobilized by FtsA or ZipA to the membrane and is located midcell (Adams and Errington, 2009). FtsA interacts with the C-terminal domain of FtsZ, which enhances initial assembly and stability of the Z-ring (Lowe and van den Ent, 2001; Adams and Errington, 2009), while ZipA, a bitopic integral inner membrane protein, interacts with the C-terminal tail of FtsZ and anchors the complex to the membrane (Hale and de Boer, 1997; Ma *et al.*, 1997). After adhering the Z-ring to the membrane, other division proteins, FtsI, FtsK, FtsW, FtsQ, FtsL, and FtsB, form the premature divisome. Then, the divisome matures through the adhesion of several proteins (PBP1B, LpoB, MltA, and EnvC) and binds to peptidoglycans and the outer membrane (Egan and Vollmer, 2013). The complete matured divisome is constricted by bending force and depolymerization of FtsZ filaments (Osawa *et al.*, 2009; Huang *et al.*, 2013) (Fig. 1, 2).

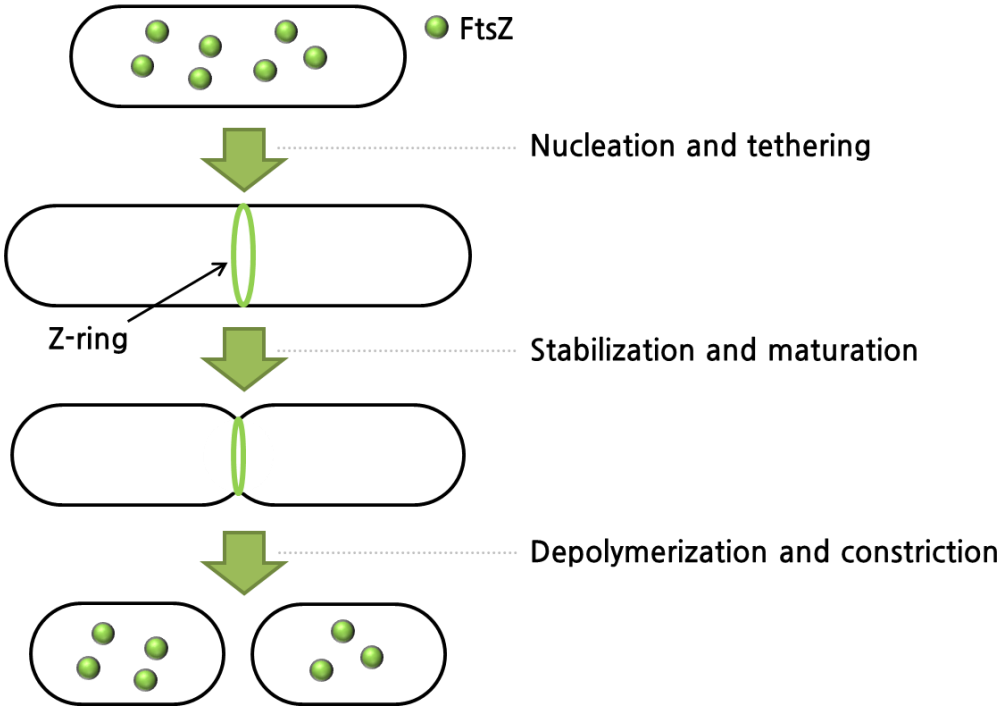

Figure 1. Scheme of FtsZ ring formation during cytokinesis

FtsZ is monomer in a new cell and FtsZ assembles at the site of division. Divisomal proteins bind to FtsZ and promote assembly to stabilize the Z-ring. In the next step of cytokinesis, Z-ring is matured by recruitment of division proteins. At the end of cytokinesis cell is divided into two daughter cells by depolymerization and constriction of Z-ring

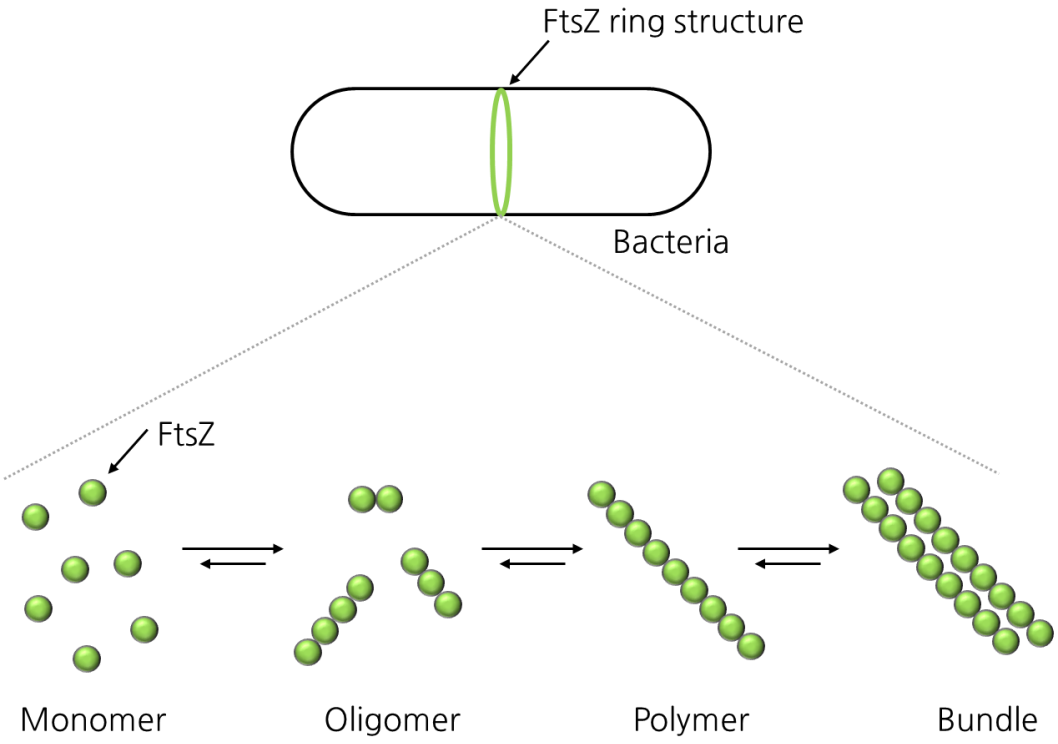

Figure 2. Polymerization of FtsZ to form Z-ring structure

FtsZ monomers assemble into oligomers, oligomers assemble into polymers, and polymers assemble into bundles and the bundles form Z-ring.

FtsZ is highly conserved in most bacteria such as eubacteria and archaea, and is also seen in chloroplasts and some primitive mitochondria (Erickson, 2009). The N-terminal domain of FtsZ, a guanosine triphosphate hydrolase (GTPase), is responsible for polymerization through the head-to-tail interaction between the guanosine triphosphate (GTP) binding pocket and the C-terminal T7 loop (de Boer *et al.*, 1992; Egan and Vollmer, 2013) (Fig. 3). FtsZ polymerization is highly regulated by several proteins, which are classified as positive or negative regulators depending on their effects. Positive regulators of FtsZ are crucial for tethering FtsZ polymers to the membrane and encouraging the formation of stable lateral interactions to assemble a mature Z-ring (Huang *et al.*, 2013). Negative regulators of FtsZ have a critical role in positioning FtsZ at the prospective site of division and for sustaining Z-ring dynamics by regulating the process of FtsZ polymer assembly and disassembly (Huang, Durand-Heredia et al., 2013). FtsZ is depolymerized by hydrolysis of GTP (Adams and Errington, 2009) (Fig.3B).

Zaps, which are FtsZ positive regulators, include ZapA, ZapB, ZapC, and ZapD and they are structurally characterized (Low *et al.*, 2004; Ebersbach *et al.*, 2008; Ortiz *et al.*, 2015; Roach *et al.*, 2016). ZapA is well known as a positive regulator of Z-ring formation, which can bind to FtsZ at the globular core directly (Galli and Gerdes, 2012). ZapC also interacts with FtsZ at the globular core and increases Z-ring stability (Huang, Durand-Heredia et al., 2013). Recently, the crystal structure of ZapC from *E. coli* showed that ZapC is a monomer composed

of two domains and it binds the FtsZ globular core rather than C-terminal tail (Schumacher *et al.*, 2016). ZapD deletion in cells resulted in no significant change in cell viability, however, decreased viability was observed in the polymerization-defective FtsZ84 (Ts) cells, suggesting that ZapD is a positive regulator of FtsZ protofilament formation (Durand-Heredia *et al.*, 2012; Huang, Durand-Heredia et al., 2013). ZapD was shown to directly bind the C-terminal tail region of FtsZ as a positive regulator (Durand-Heredia, Rivkin et al., 2012) and ZapD might form dimer to connect FtsZ bundles (Fig. 4A). ZapD decreases GTPase activity of FtsZ by binding C-terminal tail of FtsZ (Fig. 4B).

Despite extensive previous studies on the architecture of the Z-ring, the molecular mechanism of how FtsZ protofilaments are assembled to form a mature Z-ring by Zap proteins is still poorly understood. Towards such an understanding, I sought to characterize the structure and function of ZapD to elucidate how ZapD promotes the assembly of FtsZ protofilaments and acts as a positive regulator of Z-ring formation. Here, I report the crystal structures of two ZapD proteins from *S. typhimurium* and *E. coli*, which share 89% amino-acid sequence identity. Several conserved residues are clustered on the concave surface of the EcZapD dimer, which is the suggested FtsZ binding site. The opposite surface of the StZapD or EcZapD dimer is rich in conserved positively charged Arg residues. The structural and biochemical studies on ZapD from *S. typhimurium* and *E. coli* suggest that the

two FtsZ binding sites of StZapD and EcZapD dimers might be responsible for binding to two FtsZ protofilaments to hold them together.

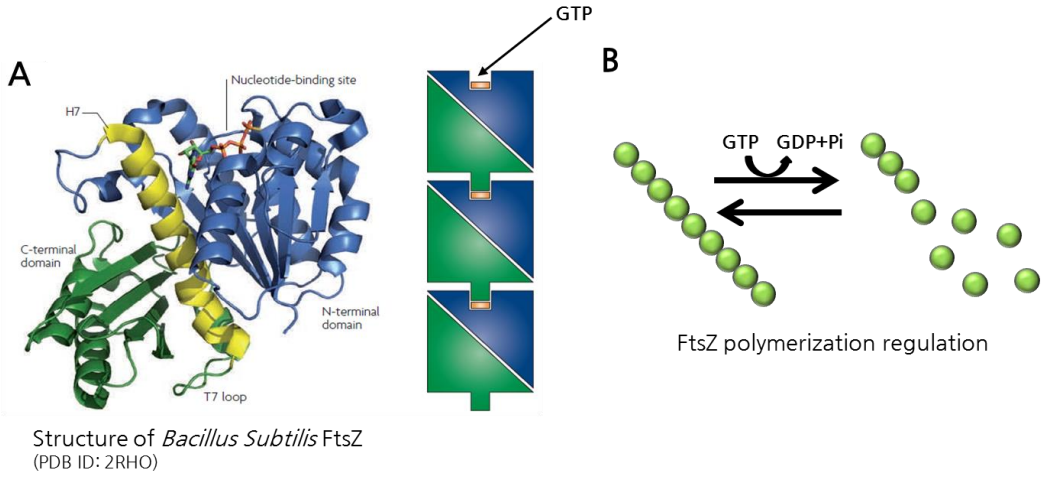

Figure 3. Structure of *Bacillus Subtilis* FtsZ and regulation of FtsZ polymerization

(A) The ribbon diagram of *Bacillus Subtilis* FtsZ. N-terminal domain is colored into blue, T7 loop is colored into yellow, and C-terminal domain is colored into green. FtsZ polymers is formed by head-to-tail interactions. (B) FtsZ is depolymerized by GTP hydrolysis.

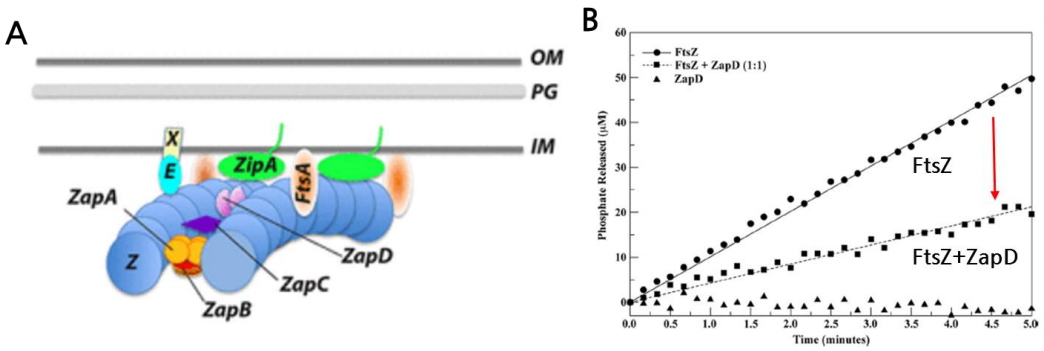

Figure 4. Putative binding model of FtsZ and Zaps

(A) Diagram of interaction between FtsZ and Zaps. ZapD is known to form dimer and bind to Ftsz to connect between FtsZ bundles. (B) GTPase assay of FtsZ and FtsZ/ZapD. ZapD decreases the GTPase activity of FtsZ.

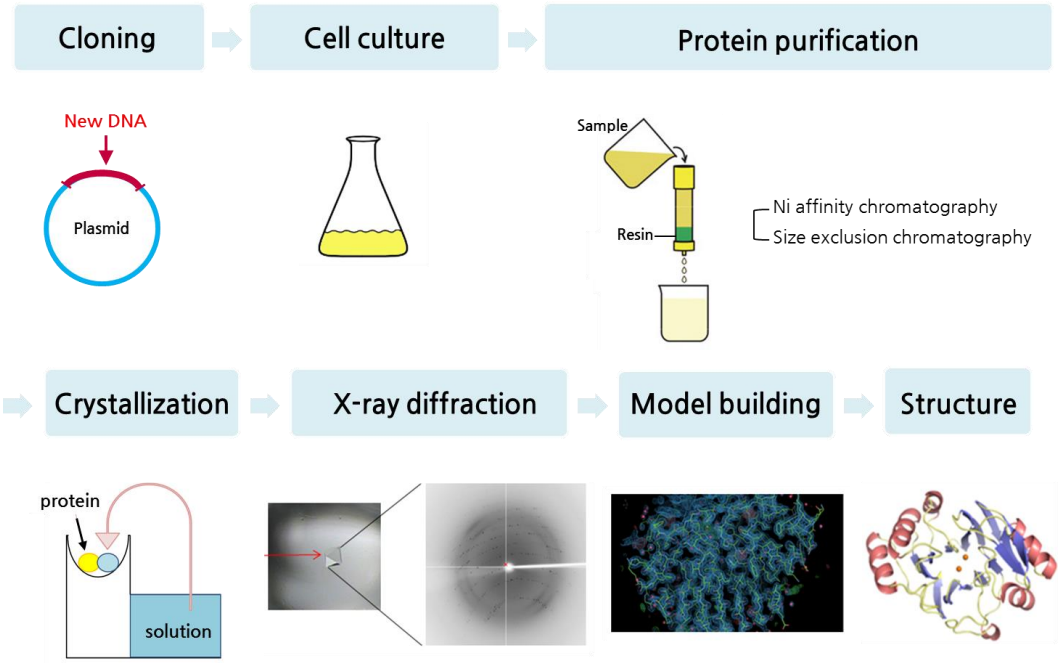

Figure 5. Overall experimental procedure

First, the target sequence is cloned into vector. The plasmid is transformed into *E.coli* cells to express proteins. The proteins from cells were purified with nickel affinity chromatography and size exclusion chromatography. The purified proteins were crystallized with about 1000 conditions. The crystals diffract with X-ray and electron density map is calculated form diffraction patterns. Then, I can solve the structure of proteins.

Ⅱ. Materials and methods

1. Cloning and protein preparation

The *S. typhimurium* $ZapD_{1–247}$ gene was amplified with polymerase chain reaction (PCR) from its genomic DNA. The forward and reverse oligonucleotide primers were 5′-C G CTA TAT **GGA TCC** C GAA AAC CTG TAT TTT CAG GGC ATG CAC ACC CAG GTC CTA TTT G-3′ and 5′-G CTA ATT **CTC GAG** TTA GCA ACA GGC CAG TTC AAA AT-3′, respectively. The bases in bold represent the BamHI and XhoI restriction enzyme cleavage sites, and underlined sequences indicate the additional Tobacco Etch Virus (TEV) protease recognition site. The amplified DNA was digested using BamHI and XhoI, and then introduced into BamHI/XhoI digested pRSFDuet–1 (Novagen) expression vector. (Fig. 6)

Methods for expression and purification of EcZapD protein (residues 2-247) are similar to previously published methods (Son and Lee, 2015). The EcZapD WT and mutants (residues 1-247, E8A, E22R, H140R, or R176A) were cloned into a pHis-parallel2 vector (Sheffield *et al.*, 1999). Constructs of EcZapD WT and EcZapD mutants with an N-terminal His-tag followed by TEV protease cleavage site (ENLYFQG) were expressed in *E. coli* strain BL21(DE3)–pLysS cells as a host, while StZapD with an N-terminal His-tag followed by TEV

protease cleavage site was expressed in *E. coli* strain BL21(DE3) cells as a host. The cells were treated with 0.5 mM isopropyl-β-D-1-thiogalactopyranoside (IPTG) to induce protein expression at 20°C for 20 h. Cells were lysed by passage through a Microfluidizer (Microfluidics, USA) in 20 mM Tris-HCl pH 7.9, 500 mM NaCl, 5 mM imidazole, and 1 mM phenylmethylsulfonyl fluoride (PMSF). The protein was purified using a Ni-sepharose affinity column, and was further purified by size exclusion chromatography (HiLoad 16/600 Superdex 75 prep grade, GE Healthcare) and stored in small aliquots at -80°C (Fig. 7).

EcFtsZ peptides (GST-FtsZ$_{367-383}$, GST-FtsZ$_{367-383}$ K380D, GST-FtsZ$_{372-383}$, and GST-FtsZ$_{367-379}$) were fused to an N-terminal GST tag followed by a TEV protease cleavage site. The GST-FtsZ$_{367-383}$ construct was amplified by PCR. The forward and reverse primers used to amplify the GST-FtsZ$_{367-383}$ construct were 5′-G CTA TAT **GGA TCC** AAA GAG CCG GAT TAT CTG GAT-3′ and 5′-G CTA ATT **CTC GAG** TTA ATC AGC TTG CTT ACG-3′, respectively. The bases in bold represent BamHI and XhoI restriction enzyme cleavage sites. Amplified DNA was digested with BamHI and XhoI and was then inserted into the BamHI/XhoI-digested expression vector pGST-parallel2 (Sheffield, Garrard et al., 1999). The plasmids were transformed into *E. coli* BL21(DE3) cells (Invitrogen), and cells harboring the plasmids were grown at 37°C until the optical density (at 600 nm) reached 0.7–1.0 in Luria Bertani (LB) broth containing 100 μg/mL ampicillin. Then, 0.5 mM IPTG was used to induce protein expression in the cells, after

which the cells were incubated for 3 h at 37°C. Cells were harvested by centrifugation at 5,000 rpm at 4°C for 20 min, and the pellet was resuspended in ice-cold lysis buffer A (20 mM Tris-HCl pH 8.0 and 200 mM NaCl) containing 1 mM PMSF. The cells were lysed using microfluidizer (Microfluidics, USA), and the lysed cells were centrifuged at 12,000 rpm (Vision V506CA rotor) at 4°C for 30 min to separate the supernatant and cell debris. The supernatant was applied to a glutathione-Sepharose column (GE Healthcare) pre-equilibrated with lysis buffer. Initially, the column was washed extensively with lysis buffer A, after which the protein was eluted with elution buffer (150 mM Tris-HCl pH 8.0 and 15 mM reduced glutathione). Further purification was performed by gel filtration on a HiLoad 16/600 Superdex 75 prep-grade column (GE Healthcare), which was equilibrated with buffer A.

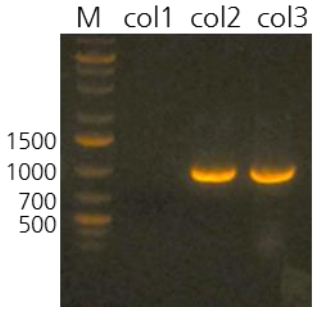

Figure 6. Colony PCR of StZapD

Agarose gel of colony PCR of StZapD. StZapD was cloned into pRSF-duet vector and was verified by using PCR with backbone primers. The StZapD colony PCR product size is about 1000bp.

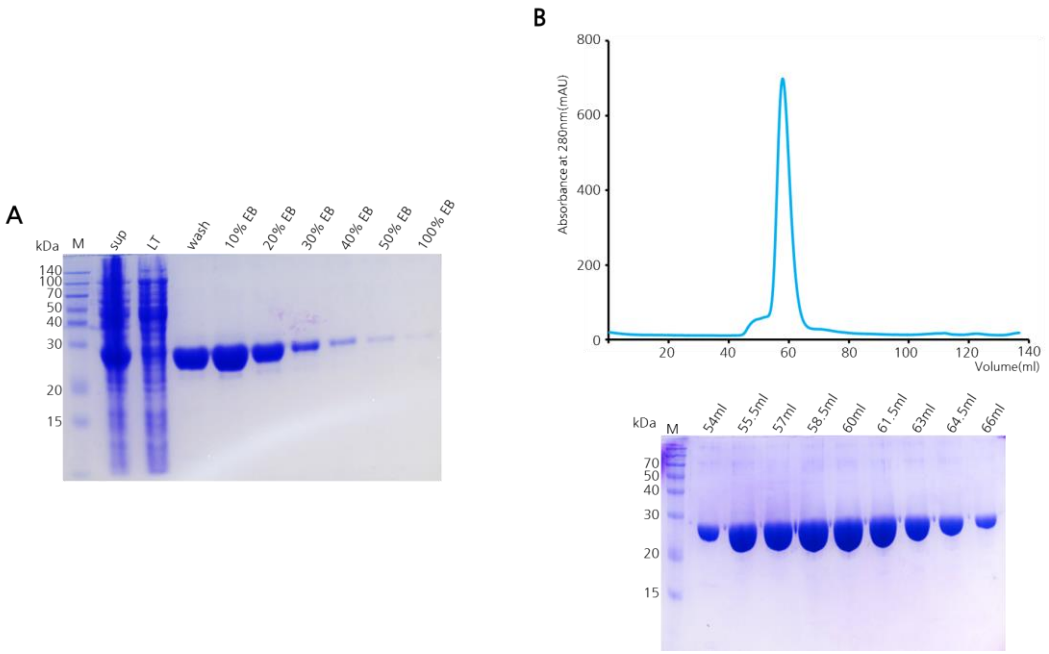

Figure 7. The purification of StZapD

(A) SDS-PAGE analysis of affinity chromatography fractions. (B) Elution profile from the Superdex-75 column chromatography and SDS-PAGE analysis of gel filtration. Elution was performed with 20 mM Tris-HCl at pH 8.0 and 200 mM NaCl.

2. Crystallization, structure determination, and refinement

The crystallization method and the data processing parameters for EcZapD (residues 2-247) has been published elsewhere (Son and Lee, 2015). The structure of EcZapD was solved by the molecular replacement method using the DUF1342 model from *Vibrio parahaemolyticus* (unknown function, PDB ID: 2OEZ) as the probe. Crystals of the StZapD (residues 1-247) were grown at 293 K using the sitting drop method by mixing 1 μl of the StZapD solution at 12 mg/mL in 20 mM Tris-HCl (pH 8.0), 200 mM NaCl, and 1 mM dithiothreitol (DTT) with 1 μl of the reservoir solution consisting of 1.1M sodium malonate, 100 mM HEPES (pH 7.5), and 0.5%(v/v) Jeffamin ED-2001 (pH7.0) (Fig. 8). Data sets were collected at 100 K in 1° oscillations at the 5C beamline of the Pohang Light Source (PLS). Crystals of StZapD diffracted to a resolution of 2.6 Å (Table 1), and the diffraction data were processed and scaled using the *HKL2000* software package (Otwinowski and Minor, 1997). The structure was solved using the molecular replacement method using the DUF1342 model as a probe. The crystal belonged to space group $P6_322$ with unit cell parameters of a = 84.2 Å, b = 84.2 Å, and c = 150.4 Å. A cross-rotational search followed by a translational search was performed using the *PHASER* program (McCoy *et al.*, 2007). Subsequent manual model building was performed using the *COOT* program (Emsley and Cowtan, 2004) and restrained refinement was carried out using the *REFMAC5* program (Murshudov *et al.*, 1997). Several rounds of model building, simulated annealing,

positional refinement, and individual B-factor refinement were performed using the *COOT* and *REFMAC5* programs. As the test data for the calculation of R_{free}, 5% of the data were randomly set aside (Brunger, 1992). The coordinates and structure factors for StZapD and EcZapD have been deposited in the Protein Data Bank under accession numbers 5GNP and 5IMJ, respectively.

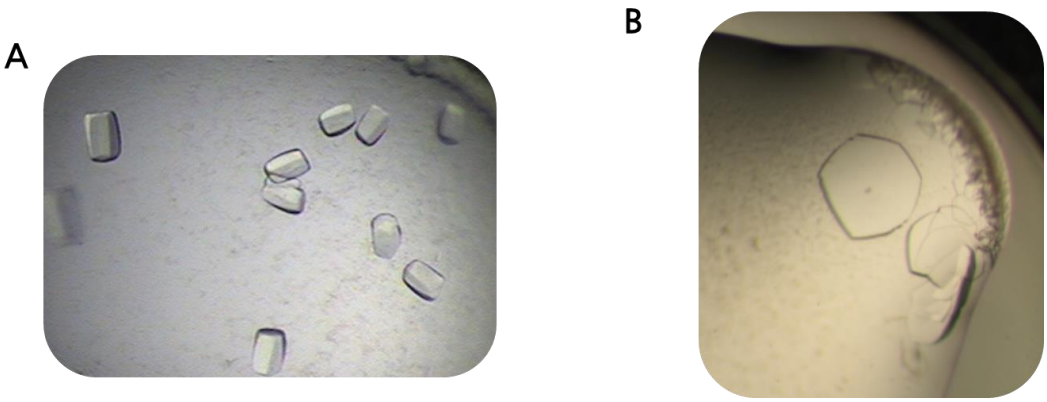

Figure 8. The crystals of EcZapD and StZapD

(A) The crystals of EcZapD were obtained using lithium sulfate as a precipitant.

(B) The crystals of StZapD were obtained using sodium malonate as a precipitant.

3. Size exclusion chromatography with multi-angle light scattering (SEC-MALS)

SEC-MALS experiments for EcZapD and StZapD were performed using a FPLC system (GE Healthcare) connected to a Wyatt MiniDAWN TREOS MALS instrument and a Wyatt Optilab rEX differential refractometer. A Superdex 200 10/300 GL (GE Healthcare) gel-filtration column pre-equilibrated with buffer A was normalized using ovalbumin protein. Proteins were injected (1 mg) at a flow rate of 0.4 mL/min. Data were analyzed using the Zimm model for static light-scattering data fitting and graphed using EASI graph with a UV peak in the ASTRA V software (Wyatt).

4. Bio-layer interferometry (BLI) measurement

BLI measurements were carried out to demonstrate binding between EcZapD (WT or mutants) and EcFtsZ (GST-FtsZ$_{367-383}$, GST-FtsZ$_{367-383}$ K380D, GST-FtsZ$_{372-383}$, or GST-FtsZ$_{367-379}$) by using a BLItz system (ForteBio, Menlo Park, CA). EcFtsZ proteins (GST-FtsZ$_{367-383}$, GST-FtsZ$_{367-383}$ K380D, GST-FtsZ$_{372-383}$, or GST-FtsZ$_{367-379}$) were immobilized on an AR2G biosensor chip surface using amine coupling in 20 mM sodium acetate (pH 4.0). The surface was activated by a 5-min immersion of N-hydroxysuccinimide (NHS)/ethyl(dimethyl-aminopropyl) carbodiimide (EDC). Subsequently, the AR2G biosensor chip was blocked by a 5-

min immersion of 1 M ethanolamine. The surface was equilibrated with buffer A. To determine whether interactions occur between EcZapD (WT, E22R, and H140R) and EcFtsZ (GST-FtsZ$_{367-383}$, GST-FtsZ$_{367-383}$ K380D, GST-FtsZ$_{372-383}$, or GST-FtsZ$_{367-379}$), the prepared AR2G biosensor chip was dipped in 35 μM protein solution in running buffer. Associations between EcZapD (WT, E22R, and H140R) and EcFtsZ (GST-FtsZ$_{367-383}$, GST-FtsZ$_{367-383}$ K380D, GST-FtsZ$_{372-383}$, or GST-FtsZ$_{367-379}$) were measured for 150 s, and dissociations were measured for 150 s.

III. Results and Discussion

1. Structure determination of EcZapD and StZapD

I have determined the crystal structures of EcZapD (residues 2–247) and StZapD (1-247) by the molecular replacement method using the DUF1342 model from *V. parahaemolyticus* (unknown function, PDB ID: 2OEZ) as the probe. To facilitate crystallization, the N-terminus of EcZapD (residue number 1) was truncated. Two monomers of EcZapD belong to the space group $P6_4$, with unit cell parameters of a = b = 109.5 Å, and c = 106.7 Å. The model of EcZapD has been refined to crystallographic R_{work} and R_{free} values of 22.7 % and 28.3% for the 35.4–3.1 Å data (Table 1). The refined EcZapD model has one dimer in an asymmetric unit with 492 residues, 5 sulfate ions, and 41 water molecules, respectively. Ramachandran plot analysis for the model showed that 86.3% and 10.2% of the non-glycine residues were in the most favored and allowed regions, and 3.5% of them were in disallowed regions (Table 1). The outlier residues are located in regions of fairly poor density.

One monomers of StZapD belong to the space group $P6_322$, with unit cell parameters of a = b = 84.2 Å, and c = 150.0 Å. The model of StZapD has been refined to crystallographic R_{work} and R_{free} values of 24.8 % and 27.7% for the 50–2.8 Å data (Table 1). The refined StZapD model has one monomer in an

asymmetric unit with 245 residues, 1 malonate ion, and 36 water molecules. Ramachandran plot analysis for the model showed that 95.9% and 3.7% of the non-glycine residues were in the most favored and allowed regions, and 0.4% of them were in disallowed regions (Table 1). The outlier residues are located in regions of fairly poor density.

Table 1. Statistics for data collection and refinement

Data set	StZapD	EcZapD
A. crystal parameters		
X-ray source	BL38B1	
X-ray wavelength (Å)	1.0000	
Space group	$P6_322$	
Unit cell parameters (Å)	a = 84.2 b = 84.2 c = 150.0	
Resolution range (Å)	50-2.8	
Total / unique reflections	107,772/8,289	
Completeness (%)	99.7 (100.0)[a]	
Average I/σ (I)	48.6 (5.9)[a]	
R_{rim}[b] (%)	11.3(62.4)[a]	
R_{pim}[c](%)	3.2(16.3)[a]	
$CC_{1/2}$[d] (%)	99.7(93.7)[a]	
B. Model refinement statistics		
Resolution range (Å)	50-2.8	35.4-3.1
R_{work} / R_{free}[e](%)	24.8 / 27.7	22.7 / 28.3
Number / average B-factor (Å^2)		
Protein nonhydrogen atoms	1,983/83.0	3,968/95.28
Water oxygen atoms	36/72.7	41/83.07
Malonate	1/100	
R.m.s. deviations from ideal		
Bond lengths (Å)	0.005	0.007
Bond angles (°)	0.927	1.208
Protein-geometry analysis		
Ramachandran favored (%)	95.9	86.3
Ramachandran allowed (%)	3.7	10.2
Ramachandran outliers (%)	0.4	3.5

Footnotes for Table 1

[a]Values in parentheses refer to the highest resolution shell (2.85–2.80 Å).

[b]$R_{rim} = \Sigma_{hkl}\{N(hkl) / [N(hkl)– 1]\}^{1/2} \Sigma_i | I_i(hkl) –<I(hkl)> | / \Sigma_{hkl}\Sigma_i I_i(hkl)$. The redundancy-independent merging R factor gives the precision of individual intensity (Diederichs and Karplus, 1997).

[c]$R_{pim} = \Sigma_{hkl}\{1 / [N(hkl) –1]\}^{1/2} \Sigma_i | I_i(hkl) –<I(hkl)> | / \Sigma_{hkl}\Sigma_i I_i(hkl)$. The precision indicating merging R factor describes the precision of the averaged intensity (Weiss, 2001).

[d]$CC_{1/2}$ is the correlation coefficient of the mean intensities between two random half-sets of data (Diederichs and Karplus, 2013).

[e]$R = \Sigma_{hkl} | |F_{obs}| – |F_{calc}| | / \Sigma_{hkl} |F_{obs}|$, where R_{free} was calculated for a randomly chosen 5% of reflections, which were not used for structure refinement and R_{work} was calculated for the remaining.

The data processing parameters for EcZapD have been described elsewhere with the reference (Son and Lee, 2015)

2. Overall structure of StZapD and its oligomeric state in solution

The StZapD monomer is composed of two domains; the N-terminal α-helices domain (NTD) and the C-terminal β-sheet domain (CTD) (Figs. 1 and 2). The NTD consists of eight α-helices, while the CTD consists of seven β strands (Figs. 1 and 2). The CTD is composed of two antiparallel β-sheets (β1-β4-β7-β2 and β5-β6-β3, respectively) facing each other (Fig. 9A). Interestingly, the N-terminal β1 is part of the C-terminal β-sheet. The asymmetric crystallization unit contains one monomer, and its dimeric assembly with approximate dimensions of 90 Å × 60 Å × 30 Å presents twofold symmetry (Fig. 9B). To unveil overall structural similarities with other known structures from PDB, a search using the DALI program was performed (Holm and Rosenstrom, 2010). It showed several structurally similar proteins including (i) cell division protein ZapD from *E. coli* (5DKO, Z-score 30) (Roach, Wroblewski et al., 2016), (ii) the DUF1342 protein (unknown function) from *V. parahaemolyticus* (2OEZ, Z-score 27), and (iii) Integron cassette protein from *V. paracholerae* (3JRT, Z-score 8.2) (Sureshan *et al.*, 2013). When I compared our StZapD refined structure with the high Z-score structures (PDB codes 5DKO, 2OEZ, and 3JRT), the r.m.s. deviations were 0.9 Å (240 Cα), 2.0 Å (240 Cα), and 5.6 Å (120 Cα) for Cα atom pairs, respectively.

The solvent-accessible surface area buried at the interface between the two monomers in the dimeric unit of StZapD was calculated by PISA (Krissinel and

Henrick, 2007), to be ~1871 $Å^2$ (13% of the monomer surface area), suggesting that StZapD may exist in solution as the dimer that is present in the crystal. To further analyze the oligomeric states of StZapD and EcZapD in solution, I measured the molecular weight of StZapD using SEC-MALS. The molecular masses of StZapD and EcZapD were 55.5 and 54.6 kDa, close to the theoretical molecular mass of dimeric StZapD (56.9 kDa) and EcZapD (56.8 kDa) in solution, respectively (Fig. 9C), indicating that the functional oligomeric state of StZapD and EcZapD in solution is dimer. It is interesting to note that other structurally characterized Zap proteins (ZapA, ZapB, and ZapC) also exist as dimer in solution, even though ZapA exists in a dimer-tetramer equilibrium in concentration-dependent manner (Low, Moncrieffe et al., 2004; Ebersbach, Galli et al., 2008; Ortiz, Kureisaite-Ciziene et al., 2015).

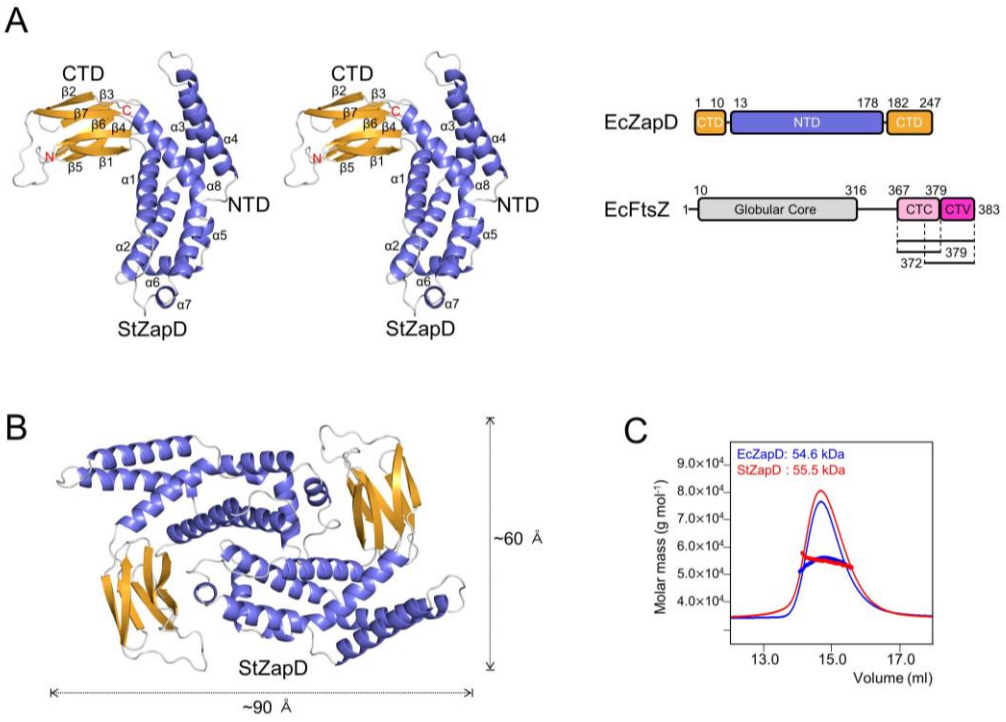

Figure 9. Overall structure of StZapD and oligomeric state in solution

(A) Stereo ribbon diagram of monomer structure of StZapD. The NTD (Nterminal domain) and CTD (Cterminal domain) are shown in light blue and gold, respectively. Loops are drawn in gray. Right panel indicates domain architectures of Ec-ZapD and EcFtsZ (Huang et al., 2016). EcFtsZ constructs used in biochemical analysis are shown in bold line. C-terminal constant region and C-terminal variable region are denoted as CTC and CTV, respectively. (B) Ribbon diagram of StZapD dimer structure. (C) The molecular weights of EcZapD and StZapD in solution were analyzed by SECMALS. The thick lines represent the measured molecular weight.

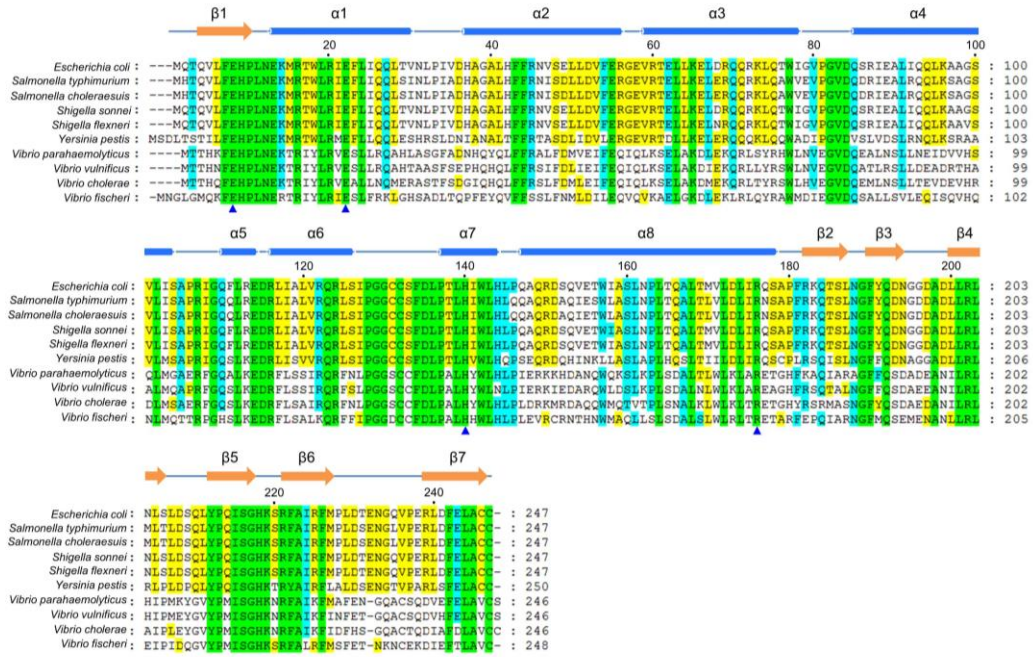

Figure 10. **Sequence alignments of StZapD with other ZapD proteins**

Multi-alignment of *E. coli* (UniProtKB/Swiss-Prot accession number J7QWY2) against ZapD from *S. typhimurium* ZapD (UniProtKB/Swiss-Prot accession number P67693), *Salmonella choleraesuis* (Uni-ProtKB/Swiss-Prot accession number Q57TB7), *Shigella sonnei* (UniProtKB/Swiss-Prot accession number Q3Z5Q7), *Shigella flexneri* (Uni-ProtKB/Swiss-Prot accession number Q83MF4), *Yersinia pestis* (UniProtKB/Swiss-Prot accession number Q8ZBH9), *Vibrio parahaemolyticus* (UniProtKB/Swiss-Prot accession number Q87LT3), *Vibrio vulnificus* (UniProtKB/Swiss-Prot accession number P67695), *Vibrio cholerae serotype O1* (UniProtKB/Swiss-Prot accession number P67694), and *Vibrio*

fischeri (UniProtKB/Swiss-Prot accession number Q5E2R1). Secondary structure elements were assigned by PyMOL (The PyMOL Molecular Graphics System, http://www.pymol.org) and every twentieth residue is marked by a black dot. Strictly (100%) and semi-conserved residues (80% and 60%) are highlighted in green, cyan, and yellow, respectively. Arrows and cylinders above the sequences denote α-helices and β-strands, respectively. Blue triangles indicate the mutation sites for EcZapD-EcFtsZ binding study.

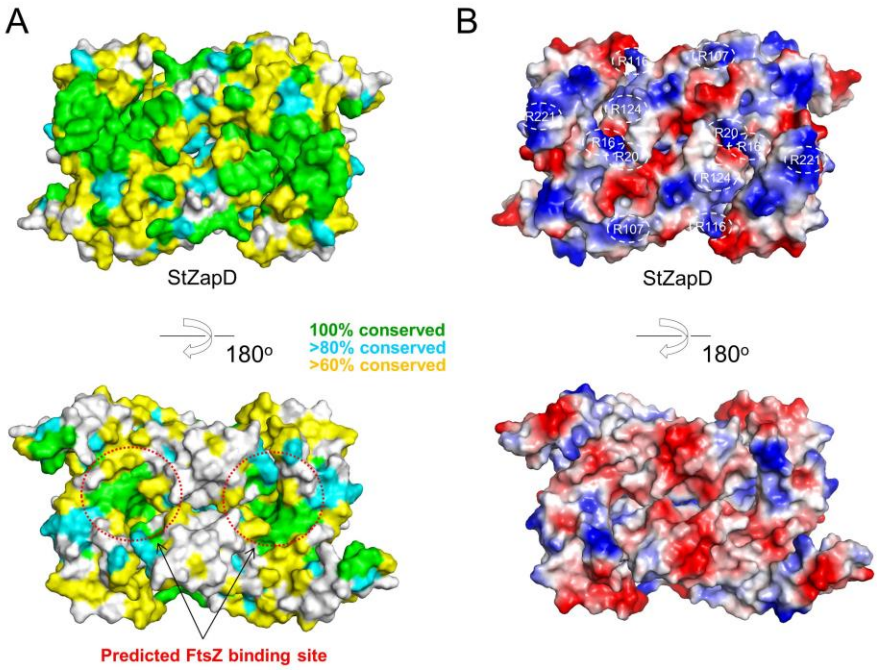

Figure 11. Surface representation of the sequence conservation and electrostatic potential of StZapD

(A) Sequence conservation mapped onto the surface of the StZapD dimer. The conserved residues are green (100%), cyan (greater than 80%), and yellow (greater than 60%). The predicted FtsZ binding sites are indicated as red dotted circles. (B) Surface representation and electrostatic potential rotated 180° around the indicated axis in comparison to the upper figure are shown below. The positions of conserved positively charged residues are indicated.

3. The binding activity of EcZapD to the C-terminal peptide of FtsZ

The C-terminal peptide of FtsZ consists of highly conserved residues and interacts with diverse FtsZ-interacting proteins, including FtsZ, ZipA, SepF, EzrA, and ZapD (Huang, Durand-Heredia et al., 2013; Son and Lee, 2013). A previous report showed that the C-terminal peptide of FtsZ could be divided into two parts—the C-terminal constant region (CTC, ^{367}KEPDYLDIPAFLR^{379} in EcZapD) consisting of conserved residues, and a C-terminal variable region (CTV, ^{380}KQAD^{383} in EcZapD) consisting of sequences diverse in length and composition (Huang, Durand-Heredia et al., 2013). To confirm the predicted function of EcZapD as an FtsZ binding protein, I attempted to measure the catalytic activity of FtsZ binding by bio-layer interferometry (BLI) experiments. BLI assays were performed by attaching C-terminal FtsZ peptides from *E. coli* (residues 367-383, 372-383, or 367-379) with GST tags (GST-FtsZ$_{367-383}$, GST-FtsZ$_{372-383}$, or GST-FtsZ$_{367-379}$) on an AR2G biosensor chip to check whether EcZapD (WT or mutants) contains peptide binding activity (Fig. 12). To ensure that the EcZapD proteins did not bind to the GST protein, but to the C-terminal FtsZ peptide specifically, a control chip containing GST only without the C-terminal FtsZ peptide was utilized. Indeed, EcZapD bound tightly to the GST-FtsZ$_{367-383}$ but not to the GST protein only (Fig. 12A and B), indicating that the interaction between EcZapD and the C-terminal

FtsZ peptide is specific. Thus, the FtsZ binding activity suggests that EcZapD is a direct modulator of FtsZ protofilaments. To check whether the N-terminal part of the CTC region is essential for EcZapD binding, I attempted to remove the five N-terminal residues (residues 367-371) of the CTC region for an EcZapD binding study. The binding affinities of EcZapD with EcFtsZ proteins (residues 367-383 and 372-383) were 4.4±0.5 and 10±0.9 μM, respectively, suggesting that residues 372-383 of FtsZ are sufficient for its binding to EcZapD (Fig. 12B). In addition, to check whether the CTV region is essential for EcZapD binding, I removed the CTV part (residues 380-383) and measured its binding affinity with EcZapD. The binding affinity was significantly lower (K_d > 2 mM) than those of other EcFtsZ constructs (residues 367-383 or 372-383), suggesting that the CTV region of FtsZ, ^{380}KQAD^{383}, is essential for binding to EcZapD (Fig. 12B). In recent study, the importance of K380 of FtsZ in the CTV region was reported (Huang et al., 2016). Thus, I performed another BLItz assay between EcFtsZ (367-383) K380D mutant and EcZapD and measured its binding affinity (K_d = 4.7±0.5 μM). It showed similar binding affinity with EcFtsZ WT (367-383) (Fig. 12B), suggesting that the mutation of K380D in EcFtsZ (367-383) is not enough to abolish the interaction with EcZapD.

4. Putative FtsZ binding sites on EcZapD and modeled structure of $EcZapD_{2-247}$-$FtsZ_{367-383}$ complex

When the molecular surface of EcZapD was drawn, two deep clefts between two monomers were found on the concave surface of EcZapD (Fig. 12). The calculated volumes of each cavity using the CASTp server (Dundas *et al.*, 2006) were 166 $Å^3$ and 98 $Å^3$, respectively. Along this cleft, several conserved residues are clustered, including Glu8, Glu22, His140, and Arg176 (Fig. 12A). This cleft appeared to be the site of FtsZ binding, thus I tried to solve the crystal structure of $EcZapD_{2-247}$-$FtsZ_{367-383}$ complex. However, I could not produce the crystal of $EcZapD_{2-247}$-$FtsZ_{367-383}$ complex despite of various screening trials. Thus, using the FlexPepDock server (London *et al.*, 2011), I have modeled the complex of $EcZapD_{2-247}$ with $FtsZ_{367-383}$ to identify the $FtsZ_{367-383}$ binding site on $EcZapD_{2-247}$ (Fig. 12A). As expected, the deep clefts between the two monomers, which were suggested to be the FtsZ binding site, were indeed responsible for $FtsZ_{367-383}$ binding. Along with the $FtsZ_{367-383}$ binding site, there were two strictly conserved residues (Glu22 and His140). Therefore, to validate this model, EcZapD mutants (E22R and H140R) were tested to determine if the mutations weaken the FtsZ binding affinity for EcZapD. Indeed, mutations of Glu22 and His140 to Arg led to slightly lower binding (K_d = 68±2.2 μM and 16±1 μM, respectively) than that with WT EcZapD (4.4±0.5 μM), suggesting the contributions of the two

conserved residues to the binding between EcZapD and EcFtsZ (Fig. 12B). I could not measure the binding affinities with the E8A and R176A mutants of $FtsZ_{367-383}$, because these proteins were expressed in insoluble forms. Based on these results, I speculated that both Glu22 and His140 contribute to the binding of EcZapD to FtsZ directly or indirectly. Although much remains to be learned about the structural architecture of FtsZ-ZapD complex and the mechanism of FtsZ protofilaments stabilization by EcZapD, the results and model presented here provide one foothold for furthering such an understanding.

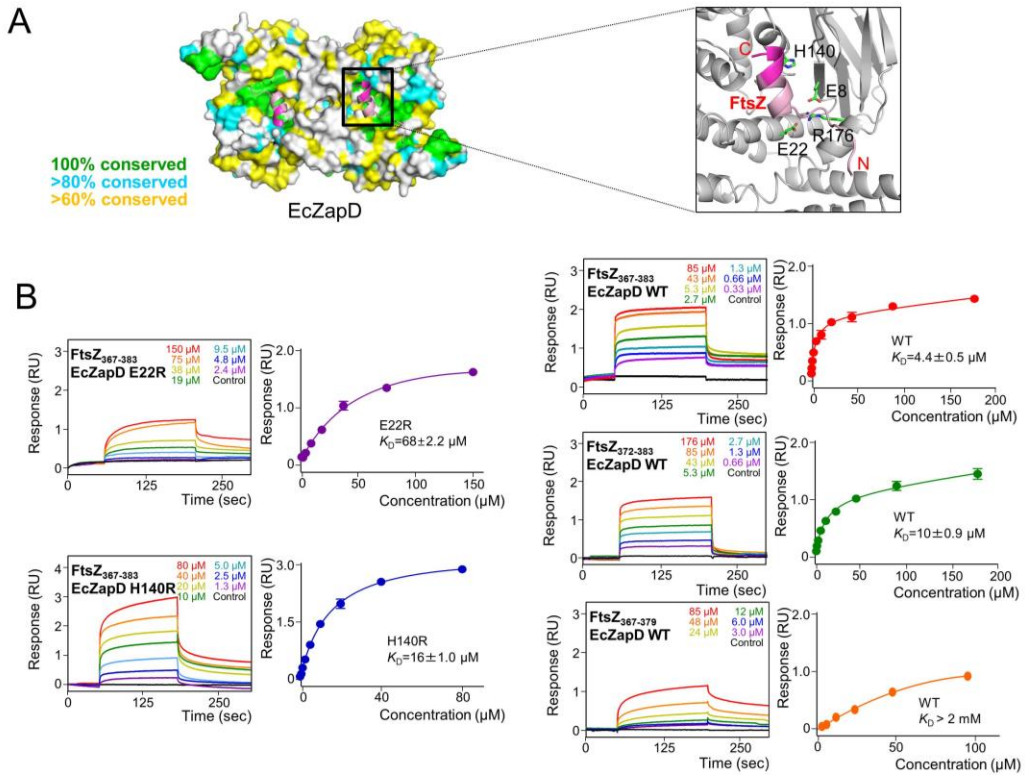

Figure 12. Modeled structure of EcZapD in complex with FtsZ peptides

(A) Modeled structure of EcZapD-FtsZ complex. Sequence conservation was mapped onto the surface of the EcZapD dimer. The conserved residues are shown in green (100%), cyan (greater than 80%), and yellow (greater than 60%). CTC and CTV regions are shown in light pink and magenta colors, respectively (Huang et al., 2016). (B) Left two panels indicate representative BLI binding sensorgrams of GST-FtsZ$_{367-383}$ with EcZapD mutants (E22R and H140R). Right three panels indicate representative BLI binding sensorgrams of EcZapD WT with GST-FtsZ$_{367-383}$, GST-FtsZ$_{372-383}$, and GST-FtsZ$_{367-379}$, respectively. The experiments were repeated three times. Each concentration of analytes is shown in a different color.

IV. References

Choi, H., Min, K., Mikami, B., Yoon, H.J. and Lee H.H. (2016) Structural and Biochemical Studies Reveal a Putative FtsZ Recognition Site on the Z-ring Stabilizer ZapD. *Mol Cells* **39(11)**, 814-820.

Adams, D.W. and Errington, J. (2009) Bacterial cell division: assembly, maintenance and disassembly of the Z ring. *Nat Rev Microbiol* **7**, 642-653.

Brunger, A.T. (1992) Free R value: a novel statistical quantity for assessing the accuracy of crystal structures. *Nature* **355**, 472-475.

de Boer, P., Crossley, R. and Rothfield, L. (1992) The essential bacterial cell-division protein FtsZ is a GTPase. *Nature* **359**, 254-256.

Diederichs, K. and Karplus, P.A. (1997) Improved R-factors for diffraction data analysis in macromolecular crystallography. *Nat Struct Biol* **4**, 269-275.

Diederichs, K. and Karplus, P.A. (2013) Better models by discarding data? *Acta Crystallogr D Biol Crystallogr* **69**, 1215-1222.

Dundas, J., Ouyang, Z., Tseng, J., Binkowski, A., Turpaz, Y. and Liang, J. (2006) CASTp: computed atlas of surface topography of proteins with structural and topographical mapping of functionally annotated residues. *Nucleic Acids Res* **34**, W116-118.

Durand-Heredia, J., Rivkin, E., Fan, G., Morales, J. and Janakiraman, A. (2012) Identification of ZapD as a cell division factor that promotes the assembly of FtsZ in Escherichia coli. *J Bacteriol* **194**, 3189-3198.

Ebersbach, G., Galli, E., Moller-Jensen, J., Lowe, J. and Gerdes, K. (2008) Novel coiled-coil cell division factor ZapB stimulates Z ring assembly and cell division. *Mol Microbiol* **68**, 720-735.

Egan, A.J. and Vollmer, W. (2013) The physiology of bacterial cell division. *Ann N Y Acad Sci* **1277**, 8-28.

Emsley, P. and Cowtan, K. (2004) Coot: model-building tools for molecular graphics. *Acta Crystallogr D Biol Crystallogr* **60**, 2126-2132.

Erickson, H.P. (2009) Modeling the physics of FtsZ assembly and force generation. *Proc Natl Acad Sci U S A* **106**, 9238-9243.

Galli, E. and Gerdes, K. (2012) FtsZ-ZapA-ZapB interactome of Escherichia coli. *J Bacteriol* **194**, 292-302.

Hale, C.A. and de Boer, P.A. (1997) Direct binding of FtsZ to ZipA, an essential component of the septal ring structure that mediates cell division in E. coli. *Cell* **88**, 175-185.

Holm, L. and Rosenstrom, P. (2010) Dali server: conservation mapping in 3D. *Nucleic Acids Res* **38**, W545-549.

Huang, K.H., Durand-Heredia, J. and Janakiraman, A. (2013) FtsZ ring stability: of bundles, tubules, crosslinks, and curves. *J Bacteriol* **195**, 1859-1868.

Huang, K.H., Mychack, A., Tchorzewski, L. and Janakiraman, A. (2016) Characterization of the FtsZ C-Terminal Variable (CTV) region in Z-Ring assembly and interaction with the Z-Ring stabilizer ZapD in *E.coli*

cytokinesis. *PLoS One* **11**, e0153337.

Krissinel, E. and Henrick, K. (2007) Inference of macromolecular assemblies from crystalline state. *J Mol Biol* **372**, 774-797.

London, N., Raveh, B., Cohen, E., Fathi, G. and Schueler-Furman, O. (2011) Rosetta FlexPepDock web server--high resolution modeling of peptide-protein interactions. *Nucleic Acids Res* **39**, W249-253.

Low, H.H., Moncrieffe, M.C. and Lowe, J. (2004) The crystal structure of ZapA and its modulation of FtsZ polymerisation. *J Mol Biol* **341**, 839-852.

Lowe, J. and van den Ent, F. (2001) Conserved sequence motif at the C-terminus of the bacterial cell-division protein FtsA. *Biochimie* **83**, 117-120.

Ma, X., Sun, Q., Wang, R., Singh, G., Jonietz, E.L. and Margolin, W. (1997) Interactions between heterologous FtsA and FtsZ proteins at the FtsZ ring. *J Bacteriol* **179**, 6788-6797.

Margolin, W. (2000) Themes and variations in prokaryotic cell division. *FEMS Microbiol Rev* **24**, 531-548.

McCoy, A.J., Grosse-Kunstleve, R.W., Adams, P.D., Winn, M.D., Storoni, L.C. and Read, R.J. (2007) Phaser crystallographic software. *J Appl Crystallogr* **40**, 658-674.

Murshudov, G.N., Vagin, A.A. and Dodson, E.J. (1997) Refinement of macromolecular structures by the maximum-likelihood method. *Acta Crystallogr D Biol Crystallogr* **53**, 240-255.

Ortiz, C., Kureisaite-Ciziene, D., Schmitz, F., McLaughlin, S.H., Vicente, M. and Lowe, J. (2015) Crystal structure of the Z-ring associated cell division protein ZapC from Escherichia coli. *FEBS Lett* **589**, 3822-3828.

Osawa, M., Anderson, D.E. and Erickson, H.P. (2009) Curved FtsZ protofilaments generate bending forces on liposome membranes. *Embo j* **28**, 3476-3484.

Otwinowski, Z. and Minor, W. (1997) Processing of X-ray diffraction data collected in oscillation mode. Macromol Crystallogr Part A 276: 307–326.

Pichoff, S. and Lutkenhaus, J. (2002) Unique and overlapping roles for ZipA and FtsA in septal ring assembly in Escherichia coli. *Embo j* **21**, 685-693.

Roach, E.J., Wroblewski, C., Seidel, L., Berezuk, A.M., Brewer, D., Kimber, M.S. and Khursigara, C.M. (2016) Structure and Mutational Analyses of Escherichia coli ZapD Reveal Charged Residues Involved in FtsZ Filament Bundling. *J Bacteriol* **198**, 1683-1693.

Schumacher, M.A., Zeng, W., Huang, K.H., Tchorzewski, L. and Janakiraman, A. (2016) Structural and Functional Analyses Reveal Insights into the Molecular Properties of the Escherichia coli Z Ring Stabilizing Protein, ZapC. *J Biol Chem* **291**, 2485-2498.

Sheffield, P., Garrard, S. and Derewenda, Z. (1999) Overcoming expression and purification problems of RhoGDI using a family of “parallel” expression vectors. *Protein expression and purification* **15**, 34-39.

Son, S.H. and Lee, H.H. (2013) The N-terminal domain of EzrA binds to the C

terminus of FtsZ to inhibit Staphylococcus aureus FtsZ polymerization. *Biochem Biophys Res Commun* **433**, 108-114.

Son, S.H. and Lee, H.H. (2015) Crystallization and preliminary X-ray crystallographic analysis of Z-ring-associated protein (ZapD) from Escherichia coli. *Acta Crystallogr F Struct Biol Commun* **71**, 194-198.

Sureshan, V., Deshpande, C.N., Boucher, Y., Koenig, J.E., Stokes, H.W., Harrop, S.J., Curmi, P.M. and Mabbutt, B.C. (2013) Integron gene cassettes: a repository of novel protein folds with distinct interaction sites. *PLoS One* **8**, e52934.

Weiss, M.S. (2001) Global indicators of X-ray data quality. *J Appl Cryst* **34**, 130−135.

국 문 초 록

튜블린 상동체인 FtsZ는 박테리아의 세포 분열에서 Z-ring을 이루는 필수 단백질이다. FtsZ는 N-말단 및 C-말단 도메인으로 이루어져 있고 C-말단의 꼬리 부분은 보존되어있다. FtsZ 프로토필라멘트와 여러 개의 Z-ring 관련 단백질(Zaps) 사이의 상호 작용은 Z-ring의 형성을 조절하는 데 필요하다. Z-ring의 양성 조절자 중 하나인 ZapD는 FtsZ의 C-말단 꼬리 부분에 직접 결합하여 세포질 분열 동안 안정한 Z-ring의 형성을 촉진한다. ZapD가 FtsZ의 C-말단 꼬리 부분과 어떻게 상호 작용하는지에 대한 구조 및 기능적 이해을 얻기 위해 Salmonella typhimurium (StZapD)와 Escherichia coli (EcZapD)로부터 ZapD 단백질의 결정 구조를 각각 2.6 및 3.1Å으로 규명했다. 예측한 FtsZ 결합 부위인 StZapD와 EcZapD 이합체의 오목한 면에 여러 보존 된 잔기가 모여있다. EcZapD-EcFtsZ의 모델링 된 구조 및 bio-layer interferometry 실험을 통해 EcZapD에서의 EcFtsZ결합 부위를 확인했다. 구조적 이해와 bio-layer interferometry 분석의 결과는 ZapD 이합체의 두 FtsZ 결합 부위가 ZapD 이합체와 두 개의 프로토필라멘트의 결합을 담당 할 수 있음을 나타낸다.

주요어: 세포분열 / 세포질분열 / FtsZ / ZapD

학번: 2015-20416